The Ribosome: Structure, Function, Antibiotics, and Cellular Interactions
Edited by R. A. Garrett, S. R. Douthwaite, A. Liljas, A. T. Matheson, P. B. Moore, and H. F. Noller

Chapter 3

Identification of Selected Ribosomal Components in Crystallographic Maps of Prokaryotic Ribosomal Subunits at Medium Resolution

ANAT BASHAN, MARTA PIOLETTI, HEIKE BARTELS, DANIELA JANELL, FRANK SCHLUENZEN, MARCO GLUEHMANN, INNA LEVIN, JOERG HARMS, HARLY A. S. HANSEN, ANTE TOCILJI, TAMAR AUERBACH, HORACIO AVILA, MARIA SIMITSOPOULOU, MOSHE PERETZ, WILLIAM S. BENNETT, ILANA AGMON, MAGGIE KESSLER, SHULAMITH WEINSTEIN, FRANÇOIS FRANCESCHI, and ADA YONATH

Several crystal types were obtained from intact or complexed ribosomal particles by systematic increase of the homogeneity of the crystalline materials prior to and after crystallization (Table 1) (Yonath et al., 1998). The crystals of the large ribosomal subunits from *Haloarcula marismortui*, H50S, diffract to the highest resolution, 2.7 Å (von Böhlen et al., 1991), but display several undesired properties (Yonath et al., 1998). In contrast, the crystals of the small (T30S) and large (T50S) subunits from *Thermus thermophilus*, which currently diffract to around 3 Å, yielded quality data even when their resolution extended only to low-resolution, 8- to 12-Å (Yonath et al., 1988; Volkmann et al., 1990).

Synchrotron radiation (SR) is required for all steps of the crystallographic analysis, due to the extremely weak diffraction power of the ribosomal crystals. It was found that a moderate SR beam causes minor crystal damage but yields only medium-resolution data. For collecting data at the higher-resolution shells, beyond 5 Å, brighter SR is required. Under these conditions the ribosomal crystals show severe radiation sensitivity even at helium stream temperatures, 15 to 25 K (Krumbholz et al., 1998; Yonath et al., 1998). Nevertheless, procedures overcoming part of the decay problem have been developed for the crystals of the thermophilic ribosomes (Schluenzen et al., 1999). For H50S, however, the situation is more complicated due to the inherent low level of isomorphism and the high heterogeneity of their crystals.

The electron density maps obtained for T30S and H50S reveal recognizable features, resembling those seen in the electron-microscopic (EM) reconstructions of the corresponding particles, obtained either by using averaging techniques of single particles or diffraction from ordered arrays. In this chapter we focus on the electron density map of the small ribosomal subunit. We show features interpreted as ribosomal proteins and rRNA and pinpoint secondary-structure elements. The use of heavy-atom markers for unbiased targeting of surface rRNA (e.g., the 3′ end of the 16S RNA) and for the localization of proteins TS11 and TS13 is highlighted. Efforts to induce controlled conformational changes within the crystals are also discussed.

Anat Bashan, Heike Bartels, Inna Levin, Moshe Peretz, Ilana Agmon, Maggie Kessler, and Shulamith Weinstein ■ Department of Structural Biology, Weizmann Institute, 76100 Rehovot, Israel. **Marta Pioletti, Horacio Avila, Maria Simitsopoulou, and François Franceschi** ■ Max Planck Institute for Molecular Genetics, Ihnestr. 73, 14195 Berlin, Germany. **Daniela Janell, Frank Schluenzen, Marco Gluehmann, Joerg Harms, Harly A. S. Hansen, Ante Tocilji, and William S. Bennett** ■ Max Planck Research Unit for Ribosomal Structure, Notkestr. 85, 22603 Hamburg, Germany. **Tamar Auerbach** ■ Department of Structural Biology, Weizmann Institute, 76100 Rehovot, Israel, and Department of Biochemistry and Pharmacology, FU-Berlin, Takustr. 3, 14195 Berlin, Germany. **Ada Yonath** ■ Department of Structural Biology, Weizmann Institute, 76100 Rehovot, Israel, and Max Planck Research Unit for Ribosomal Structure, Notkestr. 85, 22603 Hamburg, Germany.

Table 1. Crystals of ribosomal particles suitable for crystallographic studies

Source	Grown form[a]	Cell dimensions (Å)	Symmetry	Resolution (Å)
T70S	MPD	524 × 524 × 306	$P4_12_12$	17–22
T70S[b]	MPD	524 × 524 × 306	$P4_12_12$	10–14
T30S-LR	MPD	407 × 407 × 170	$P4_12_12$	9–12
T30S-HR	MPD	407 × 407 × 170	$P4_12_12$	3.0
T50S	AS	495 × 495 × 196	$P4_12_12$	3.4
H50S	PEG	211 × 300 × 567	$C222_1$	2.7

[a] Crystals were grown by vapor diffusion in hanging drops from solutions containing methyl-pentane-diol (MPD), ammonium sulfate (AS), or polyethylene glycol (PEG).
[b] A complex of T70S, 2 molecules of Phe-tRNA^{Phe}, and an oligomer of 35 uridines (as mRNA).

THE CONFORMATION OF THE CRYSTALLINE 30S SUBUNITS

The small ribosomal subunits exhibit the lowest level of stability and the highest level of flexibility among the ribosomal particles (Berkovitch-Yellin et al., 1992; Lata et al., 1996; Harms et al., 1999; Gabashvili et al., 1999). Multiple conformational states were suggested to account for the inconsistencies in locations of selected components revealed by surface probing (Alexander et al., 1994) or by monitoring the ribosomal activity (Weller and Hill, 1992). Indeed, the early T30S crystals (Yonath et al., 1988; Trakhanov et al., 1989) yielded satisfactory data only to 10- to 12-Å resolution (Schluenzen et al., 1995).

Marked improvement was obtained by employing milder conditions for ribosome purification and by inducing conformational adaptations prior to the crystallization or within the crystals, exploiting selected additives or controlled heating. Careful interplay between multimetal clusters, organometallic compounds, and heavy-atom salts yielded four derivatives located in over 50 sites. These, after extensive cross-verifications, led to a 7.2-Å electron density map (Harms et al., 1999) that was later extended to 5.5-Å resolution by the addition of a heavy-atom derivative that diffracts to higher resolution as well as by stepwise addition of phase improvement obtained by density modification procedures (Schluenzen et al., 1999).

Both the 7.2- and 5-Å maps contain morphologies remarkably similar to most of the EM reconstructions of the small subunits with their recognizable features (Fig. 1), showing the traditional division of the 30S subunit into three main parts: a head, a rather narrow neck, and a bulky lower body (Stark et al., 1995; Frank et al., 1995; Lata et al., 1996; Gabashvili et al., 1999). Some regions of the map show tertiary organization resembling the arrangements of RNA duplexes postulated by incorporating biochemical, footprinting, and cross-linking data within envelopes obtained by cryo-EM (Mueller and Brimacombe, 1997).

At the current resolution the accurate definition of the borders of the particle is prone to misinterpretation. Therefore, the relationships between the available EM reconstructions of the different conformers of the 30S subunit (Stark et al., 1995; Gabashvili et al., 1999; Harms et al., 1999) and the crystallographic map were examined. This turned out to be a rather complicated task, since neither of the available models seemed to fully fit the shape obtained by X-ray crystallography (Fig. 1). Conformational changes induced by the crystallization conditions cannot be excluded. However, since the crystalline particles exhibit functional activity within the crystals, it is reasonable to assume that these conformational changes are neither extensive nor destructive.

Reasonable agreement of the packing arrangements and moderate scores were obtained in molecular-replacement searches with cryo-EM reconstructions of the thermophilic particles, namely, that obtained from the T30S particles from the same batch that was used for crystallization and that computed by removing the density assigned to the T50S subunit within the three-dimensional reconstruction of the T70S ribosome (Harms et al., 1999). Slightly higher scores resulted when the reconstruction of *E. coli* 30S (E30S) at a conformation close to that assigned to the small subunit within the E70S ribosomes to which fMet-tRNA was bound (Malhotra et al., 1998) was used. This solution (correlation coefficients calculated with structure factors, 71%; correlation coefficients calculated with agreement factors, 39.2%; and ratios between the correlation coefficient of the best solution and that of the following one, 1.04) was treated as a mask for solvent flattening of the multiple isomorphous replacement (MIR) maps. This synthesis resulted in a map with higher connectivity and more-distinct features, but did not remove the discrepancies between the crystalline and the EM-reconstructed views.

Despite the discrepancies discussed above, all molecular-replacement searches gave rise to two common features: a large internal solvent region and pairing of the 30S particles around the twofold axis.

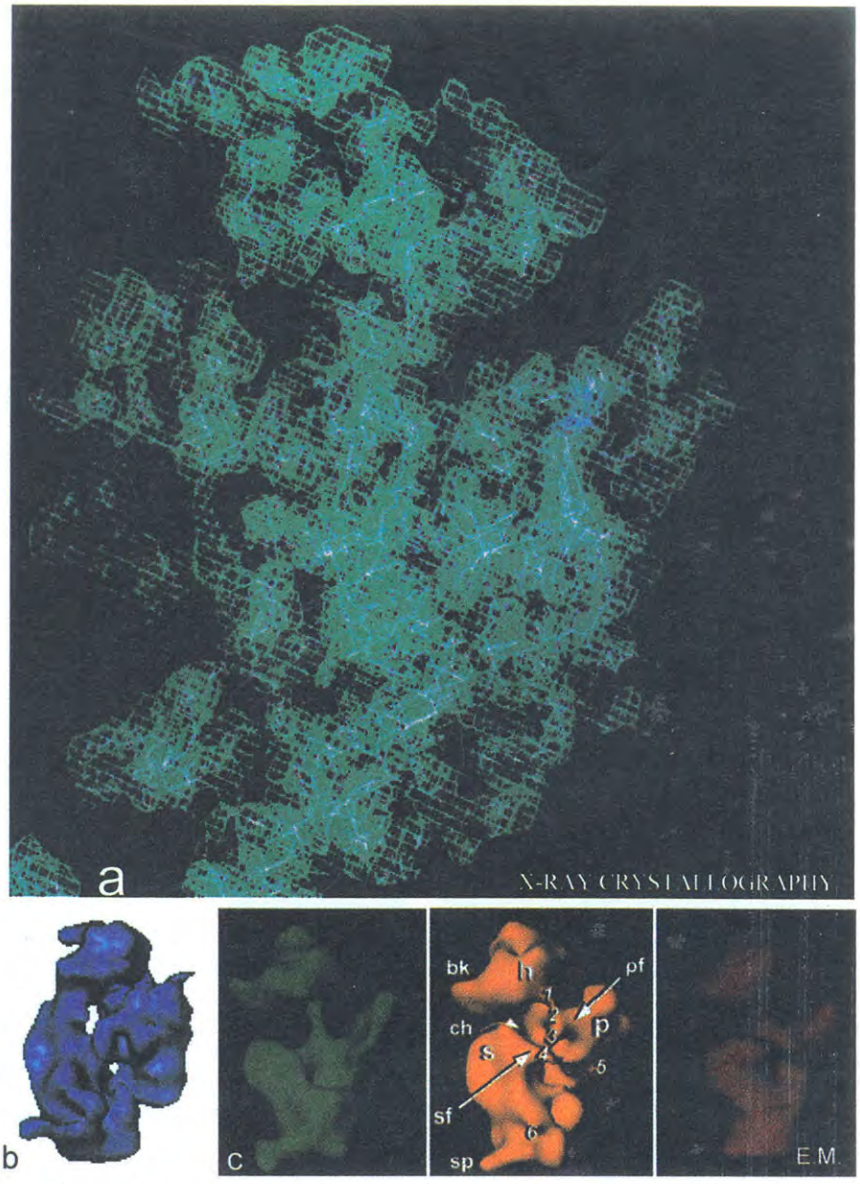

Figure 1. (a) The 7.2-Å map of T30S, contoured at 1.3 σ and sectioned in a direction allowing comparison to the available EM reconstructions of the T70S-bound T30S particle (van Heel and Stark, unpublished) (b) and the E30S conformer resembling that seen in 70S ribosomes to which fMet-tRNA is bound (Gabashvili et al., 1999) (c). A total of 21,000 unique reflections at the range 7.2 to 12.5 Å were included. Four derivatives were used: mercury acetate, platinum tetrachloride, Ta_6Br_{14}, and $C_2Hg_6N_2O_8$. The final statistics were as follows: FOM = 0.671; phasing power = 1.4, R_{cullis} = 0.8 to 0.91. For the 5-Å map, phase information was added from an additional heavy-atom derivative, methylmercury acetate, that was bound to the particle prior to crystallization. A total of 62,037 reflections were used. The final FOM was 0.77, and the phasing power was 1.25. bk, beak; ch, channel; sp, spur; sf, shoulder finger; pf, platform finger; s, shoulder; h, head; p, platform.

The pairing contacts are fairly extensive, so that they are maintained even after the crystals are carefully dissolved. Thus, the majority of the particles seen in samples of dissolved crystals are pairs with a typical butterfly-like shape. So far, it has not been possible to assign functional relevance to the crystallographic pairing or to the previously observed pairing (Zamir et al., 1971; Guerin and Hayes, 1987). It is conceivable that these extensive particle interactions emulate some of the contacts in which the small subunit is involved at the intra-ribosomal subunit interface and/or the contacts needed for the formation of intermediates along the path of the translation cycle.

SELECTED COMPONENTS WITHIN THE 30S SUBUNIT

The 7.2-Å map of T30S reveals a wealth of internal features. These include dense elongated chains that span the 30S particle in various directions and show features similar to those detected in nucleosome core particles at comparable resolution (Richmond et al., 1984). Some of these are traceable either as RNA duplexes or as single strands. The globular regions of lower density could be assigned to folds observed in isolated ribosomal proteins as determined by nuclear magnetic resonance (NMR) and crystallography at atomic resolution.

Uncertainties are associated with the placement of structures determined for isolated ribosomal components into medium- or low-resolution maps of entire ribosomal particles. These stem from the ambiguities which are likely to accompany the fitting of frequently occurring structural motifs (Liljas and Al-Karadaghi, 1997; Ramakrishnan and White, 1998) into medium-resolution maps. An additional source of uncertainties is connected to the long-lasting question of whether the structures determined for individual ribosomal components can represent the conformation within the ribosome. Certainly the conformational variability of the isolated components is not negligible, and the in situ conformations of the individual ribosomal components may be influenced by their proximity to other ribosomal proteins or rRNA. Nevertheless, structural studies showed in several cases that conformation variability is limited to the flexible part of the molecule (Clemons et al., 1998; Draper and Reynaldo, 1999). In addition, in one case the crystal structures of a ribosomal protein from two different sources are almost identical (Hosaka et al., 1997; Wimberly et al., 1997).

The elongated continuous dense regions which span the particle in various directions were traced as RNA chains (Fig. 2). The fitting of the RNA was performed mostly manually, using segments of 6 to 12 bases at a time. In several cases, regions of higher density, interpretable as the backbone phosphates, were detected within the elongated chains. About a third of the regions assigned to the 16S RNA were fitted, with varying levels of confidence. Most of these regions display the known duplex conformation, but in several cases we encountered duplexes with conformations that deviated from that of canonical double helices. Automated searches with the program ESSENS (Jones et al., 1991) were also employed, with UUAGCU as a 6-base template for single-stranded RNA of a duplex conformation and the same segment together with its counterpart, AAUCGA, to represent the duplexes. The segment CGCUACAA in the conformation of bases 69 to 76 of *Saccharomyces cerevisiae* initiator tRNA (Basavappa and Sigler, 1991) was used as a representative of relatively long stretches, and the anticodon region from the same molecule was the template for curved conformations. Although these searches led to some impressive assignments, the risk involved in their exclusive employment cannot be overlooked. Since the ribosomes contain repeating motifs of RNA, such searches are bound to suggest multiple solutions, with no provision for making the best choice. Therefore, manual assignment was preferred.

The globular regions seen in the maps, most of which are of lower average density (e.g., 0.8 σ vs. 1.1 σ for RNA), were found appropriate to accommodate ribosomal proteins. Keeping in mind that such assignments are only partially justified, the known structures of the ribosomal proteins were positioned in the map. This was performed according to the locations suggested in earlier studies, based on immuno-EM, neutron scattering, cross-linking, and modeling (Stöffler and Stöffler-Meilicke, 1986; Capel et al., 1988; Mueller and Brimacombe, 1997). The main chain coordinates, as determined by X-ray crystallography or NMR for the isolated proteins at high resolution, were used as templates.

A large fraction of protein S5 (Ramakrishnan and White, 1992) is made of beta sheets, features that are not readily detectable at medium resolution. Nevertheless, it could be fitted in the 7.2-Å map (Fig. 3). Of interest are the contacts that this protein makes with its neighborhood, which is clearly separated from its own region. This protein is of special interest for our studies, as it is being used as a vehicle for the introduction of a relatively large number of selenium atoms into the small subunit for multiwavelength anomalous dispersion phasing at high resolution (Auerbach et al., in press). Proteins S6 (Lindhal, 1994), S8 (Davies et al., 1996; Nevskaya et al., 1998), and S17 (Golden et al., 1993) were also fitted manually. However, the searches for locations suita-

Figure 2. RNA chains fitted into the 7.2-Å map of T30S (contour levels, 1.25 σ). Except for those shown in the lower right two panels, all of the chains were fitted manually, using building blocks of the canonical A-form RNA duplex (mainly 5 by 2 bases). The two views shown at the lower right were located semi-automatically, using as building blocks the CCA end of the tRNA molecule (Basavappa and Sigler, 1991). The large sphere shown in the center right panel between two helical regions represents a heavy-atom cluster.

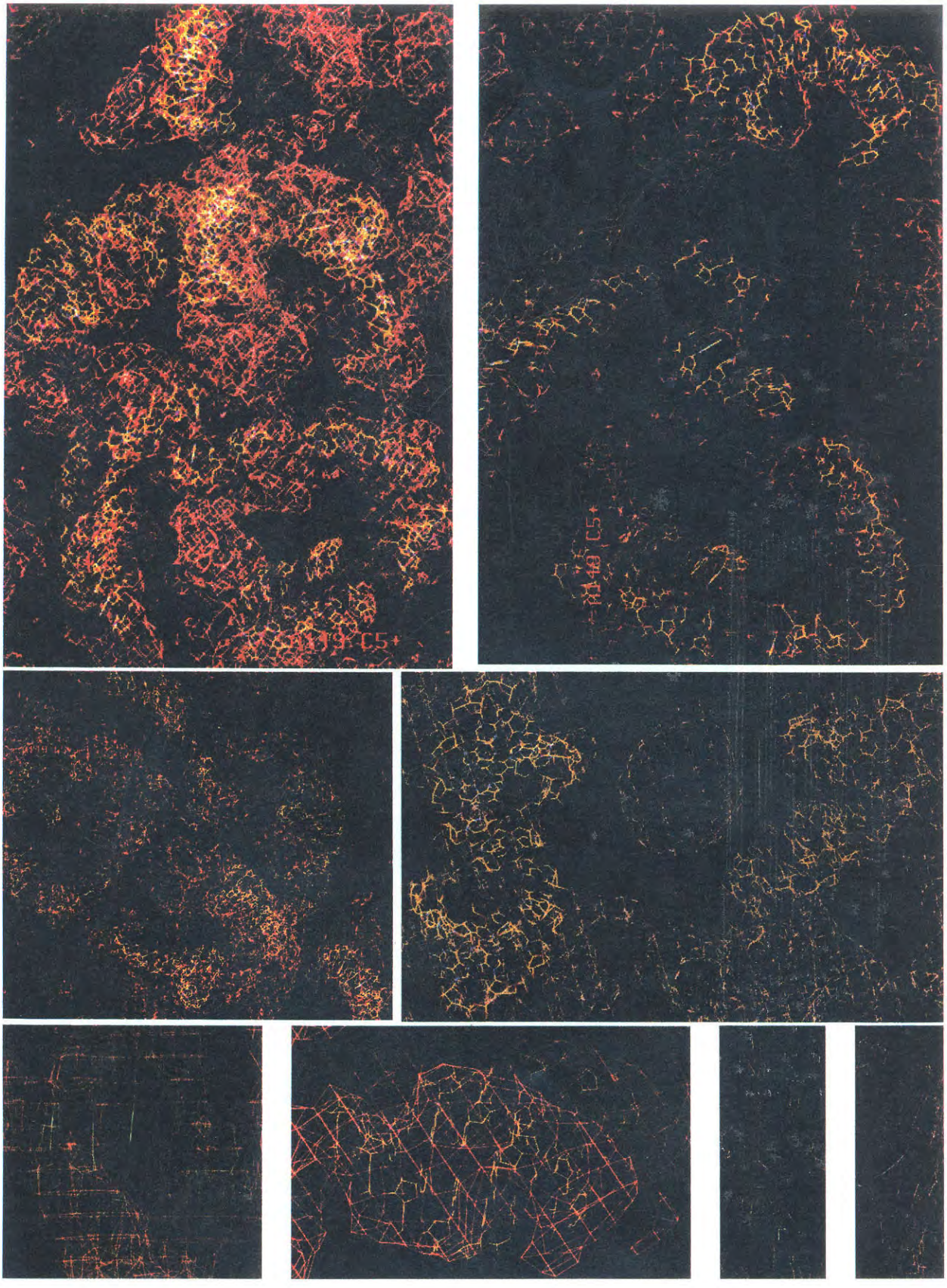
C5+
C5+

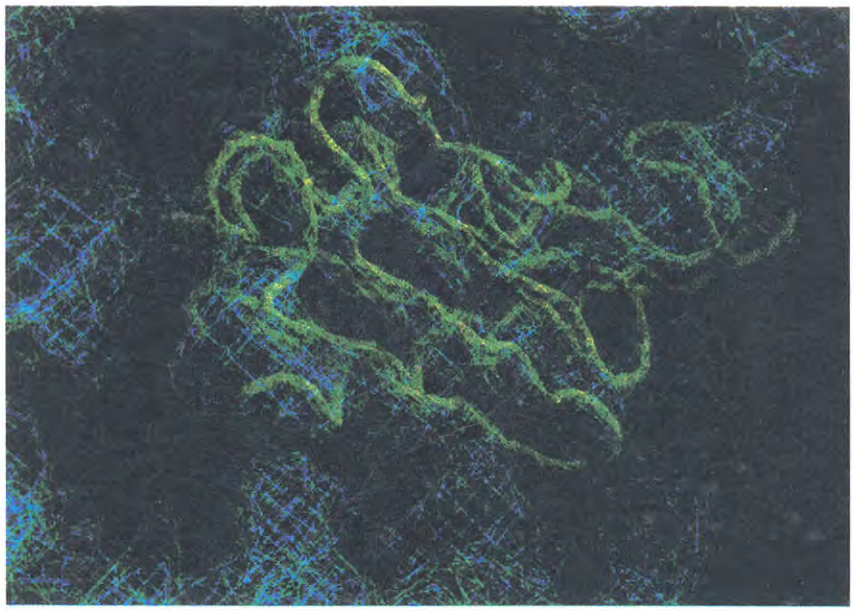

Figure 3. The main chain of the RNA binding domain of the X-ray-determined structure of protein TS5 (shown in yellow-green) overlaid on the 7.2-Å map (contoured at a signal-to-noise ratio of 0.8 [dark green] and at 1.3 σ [blue]). Note that a fair portion of the protein surface is in contact with other prominent features.

ble to host the RNA segments which interact with them were conducted in a semiautomatic fashion. Since no severe collisions were detected, these combined fitting experiments seem to be quite reliable.

The positioning of protein S7, the structure of which was determined by using two bacterial sources, *Bacillus stearothermophilus* and *T. thermophilus* (Hosaka et al., 1997; Wimberly et al., 1997) was performed manually, based on its postulated position (Tanaka et al., 1998). As mentioned above, the RNA duplexes were positioned automatically. These searches revealed a short RNA duplex contacting protein S7 (Fig. 4) that separates into its two strands once it leaves the vicinity of the protein. Interestingly, although the fitting of the protein was performed with only the main chain, the automatic search positioned the RNA so that there is sufficient room for the protein side chains.

S15 is a protein whose structure was determined by NMR and by X-ray crystallography and was shown to possess a fair amount of flexibility at a specific hinge (Clemons et al., 1998). This protein is built of three well-packed alpha-helical chains and one helix, which exhibits structural flexibility. The tentative location suggested for this protein accommodates the main helices well, but less density was found at the location where the flexible arm should be positioned if the crystallographic structure determined in isolation was maintained within the ribosomes (Schluenzen et al., 1999). Therefore, it seems that the structure determined by NMR is closer to the in situ conformation of this protein.

Inspection of the interactions among the various ribosomal components revealed several architectural elements with significant diversity in their modes of recognition, as found for smaller protein-RNA complexes (summarized by Cusack, 1999, and Draper and Reynaldo, 1999). For example, hints of the provision of support by ribosomal proteins for the stabilization of the three-dimensional fold of the rRNA chains were detected in several locations on the map.

Comparisons between the 7.2- and the 5-Å maps showed that the extension of the resolution added some detail (Schluenzen et al., 1999), but its quality is still not sufficient for reliable interpretation at the molecular level. For that, higher resolution and improved phases are essential. As we recently identified several heavy-atom derivatives that diffract to 3.5-Å and seem to possess suitable phasing power, further interpretation has been deferred to later stages.

STRUCTURAL MARKERS TARGETED TO PREDETERMINED SITES

To facilitate unbiased map interpretation, markers inserted in predetermined sites are being exploited. These are composed of heavy-atom compounds, attached either directly to the T30S particle or through carriers that bind to the ribosomal

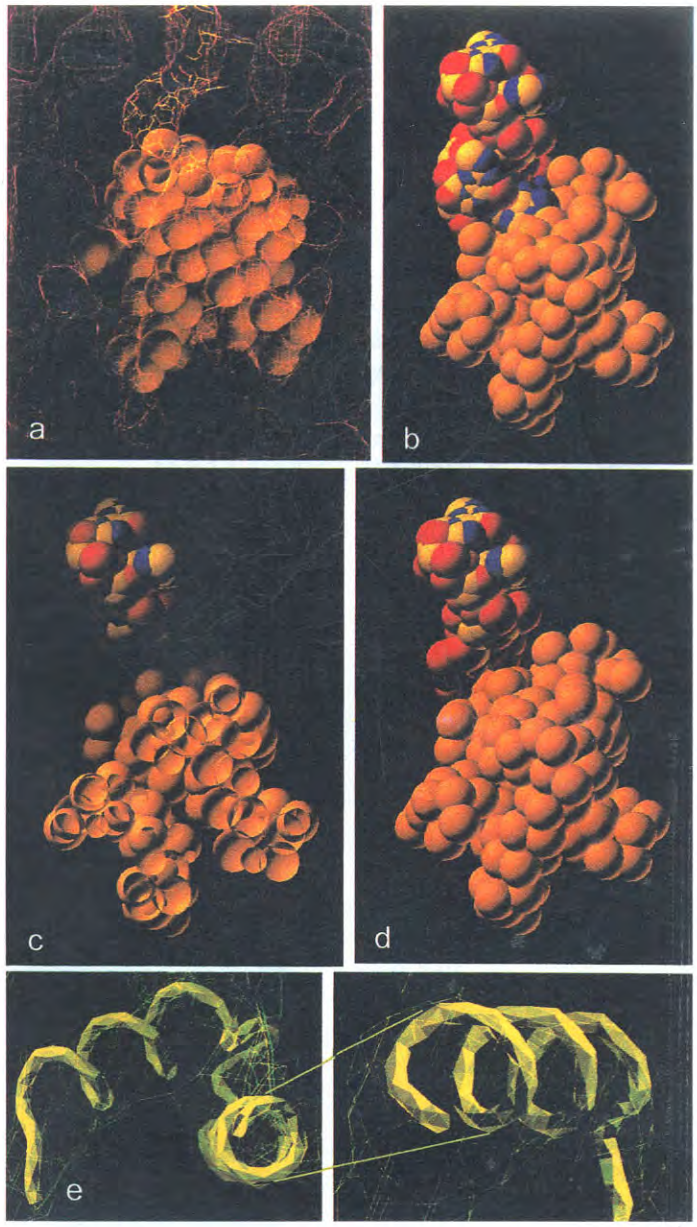

Figure 4. (a to d) About two-thirds of the backbone of protein TS7 fitted into the 7.2-Å map. The remaining third has been removed for clarity. Each dark-yellow sphere represents an amino acid. All atoms of the RNA chains are shown. (a and b) Space-filling presentation of TS7 surrounded by several features, among which one was fitted as an RNA duplex of 2 by 6 bases (shown as sticks in panel a and as a space-filling model in panel b. (c and d) Representations similar to that in panel b, but half a duplex has been removed, and a slice of it is shown, highlighting the contacts between the proteins and the RNA and the space available for the protein side chains (not shown). (e) The quality of the fitting is shown by a ribbon representing the main chain.

particles with high affinity. Candidates for carriers may be antibiotics, cDNA oligomers, charged tRNA molecules, or factors participating in the translation process, and for heavy atoms they are medium-size materials, such as tetrakis(acetoxymercuri)-methane (TAMM), a rather compact compound of four Hg atoms, and a tetrairidium cluster. The latter is composed of an internal core of four iridium atoms, with a diameter of 4.8 Å (Jahn, 1989), surrounded by a shell of organic moieties of chemical composition similar to that of proteins. To reduce the potential flexibility of this marker, its bridging arm was designed with a minimal length and maximal stability. It is slightly longer than the longest amino acid side

chain and contains an amide bond. Hence, the expectations for local, rather rigid conformations are legitimate.

Surface Ribosomal Proteins

Labeling studies showed one fully and one partially exposed SH group (Sagi et al., 1995) belonging to proteins TS11 (residue 119) and TS13 (residue 84) (Wada et al., 1999). These were used for cluster binding prior to crystallization. The crystals obtained from the modified T30S particles diffract to 4.5-Å resolution and are isomorphous with the native ones, indicating that in the crystals the motion of the cluster bridging arm is limited, as frequently happens to long side chains in proteins. As expected, the attachment of 1 to 2 equivalents of the tetrairidium cluster yielded a weak derivative, albeit a suitable marker. Thus, two prominent peaks were revealed in difference Fourier maps, constructed with the MIR phases of T30S (Weinstein et al., 1999). These were found to be in accord with the locations suggested by noncrystallographic studies. The minor site is located on the particle's upper part (the head), in a position similar to that of protein S13, as revealed by immuno-EM (Stöffler and Stöffler-Meilicke, 1986), neutron scattering (Capel et al., 1988), and modeling (Mueller and Brimacombe, 1997). The major site, assigned as the cysteine of TS11, is located at the central part of the particle, in a position roughly compatible with that suggested by immuno-EM for protein S11 in E30S as well as by modeling the ribosomal components within cryo-EM reconstructions. However, it deviates by approximately 35 Å from the position assigned to the center of mass of this protein according to neutron scattering and contrast variation. Since the tetrairidium cluster and immuno-EM target the surfaces of the ribosomal particles, whereas the triangulation method approximates the positions of the centers of mass of the ribosomal proteins, such deviation is tolerable. In fact, it is smaller than the inconsistencies of 65 Å between neutron-scattering triangulation studies and those exploiting cDNA for the localization of ribosomal components (Alexander et al., 1994).

cDNA

cDNA oligomers are being exploited for the derivatization of ribosomal crystals and for flagging the locations of the rRNA regions targeted by them, benefiting from earlier attempts at mapping the surface *E. coli* RNA in solution (Tapprich and Hill, 1986; Oakes et al., 1986; Camp and Hill, 1987; Ricker and Kaji, 1991; Hill et al., 1988; Weller and Hill, 1992; Alexander et al., 1994). In these studies synthetic oligodeoxynucleotide probes, complementary to specific rRNA, were hybridized with ribosomal particles, and alterations in activity, binding, and recognition were monitored. We chose the sequences according to their affinities and specificities, based on previous measurements carried out on T30S particles in solution. The lengths of the oligomers (10 to 22 nucleotides) were designed to increase the stability of the expected hybrid double helix.

Cocrystallization and soaking were employed, although such long heavy-atom carriers (they may reach 70 Å) are not commonly used in protein crystallography because of space limitations. In fact, soaking is preferable, since the hybridization, which is an equilibrium process, can be terminated by the shock freezing needed for data collection once it is assumed that all hybrids have been formed. A procedure leading to efficient binding has been developed. First, unmodified oligomers are diffused into native T30S crystals. Their influence on the internal order of the crystals is used to indicate whether the region with which they were supposed to interact is involved in the crystal network or exposed to the solvent. The oligomers that do not cause a substantial resolution drop are modified by heavy atoms, either in their cytidines or at their terminal phosphates. Alternatively, the heavy atoms are attached to thiolated nucleotides. The degree of hybridization of the heavy-atom-modified DNA oligomers is tested in solution, and those that display high affinity are used either for soaking experiments or for hybridization in solution and subsequent cocrystallization (Auerbach et al., in press).

Over a dozen cDNA oligomers were tested, targeting seven regions in the 16S RNA. Among them, those matching the 3′ end of the 16S RNA, as well as two regions near helix 41 (nomenclature adopted from Brimacomb [1995]), did not cause crystal damage, allowing data collection to 3.5 to 3.9 Å. Those directed to the 5′ end and to helix 21 caused a drop in resolution to 6 to 7 Å but yielded data with reasonable quality. The oligomer complementary to the 3′ end (AGAAAGGAGGTGATC) was used for derivatization after the addition of three 6-thio-G, forming a probe with three potential heavy-metal binders. Three TAMM molecules were bound quantitatively via one of their SH groups to each of the three thiolated guanidines. The unbound Hg atoms of the TAMM molecules were masked by small compounds, such as cysteine, prior to binding to the DNA oligomer. Crystallographic analysis led to the location of the TAMM compound in a difference Fourier map, using the 7.2-Å MIR phases. Thus, the proximity of

the location of the 3′ end of the 16S RNA was determined (Fig. 5).

FUNCTIONAL ACTIVATION IN PRE- AND POSTCRYSTALLIZATION STATES

The solvent content of the ribosomal crystals, 50 to 75%, falls within the range observed for other macromolecules. However, the distribution of the solvent regions is rather unusual. Sizable continuous solvent regions, with dimensions that may reach over 200 Å, were detected in the maps of T30S, T50S, and H50S (Yonath et al., 1998; Harms et al., 1999). In the crystals of H50S the unusually large continuous solvent region is rather loosely held by one interparticle contact area, leading to the undesired properties of this crystal form. In contrast, the bulky solvent within the crystals of T30S and T50S, over 200 Å in their longer dimension, could be exploited for their improvement. Thus, although in general conformational changes are not induced within crystals of biological macromolecules, because of the limited possibilities of motion imposed by the crystal network, the ribosomal particles could be reactivated within the crystals. In this way the frequency of obtaining high-quality crystals was increased significantly.

Figure 5. The suggested locations of the 3′ end of the 16S RNA (yellow-green) as detected by the Fourier method overlaid on the part of the 7.2-Å map assigned to T30S.

The Small Ribosomal Subunit

For T30S, high-quality crystals were obtained by activation of the ribosomal particles while in the crystals. With the goal of increasing the proportion of the particles that do not deviate from the preferred crystal conformation (shown to be close to that of active conformers), we are increasing the homogeneity by controlled heating (Zamir et al., 1971). Consequently, increasing proportions of crystals diffracting to around 3 Å were obtained under conditions originally found to yield crystals of moderate resolution, i.e., 4 to 4.5 Å. Along these lines, improvement of crystal quality was also achieved when crystallizing T30S particles trapped chemically at their activation state prior to crystallization or complexed with antibiotics, such as edeine (Szer and Kurylo-Borowska, 1972), known to "freeze" the 30S subunits at a particular conformational state (Moazed and Noller, 1987).

The Large Ribosomal Subunit

Among the numerous crystal forms that were obtained from large ribosomal subunits (Berkovitch-Yellin et al., 1992), two seem to be suitable for crystallographic studies. These are crystals of T50S, which yield high-quality diffraction data but until recently diffracted only to low resolution, 9 to 10 Å (Volkmann et al., 1990), and those of H50S, which give rise to rather problematic data that extend to 2.7 Å (von Böhlen et al., 1991). Owing to the undesirable properties of the latter crystals, i.e., their severe sensitivity to X-ray irradiation and their extremely low level of isomorphism, despite intensive studies carried out by us (Yonath and Franceschi, 1998; Yonath et al., 1998) as well as by others (Ban et al., 1998), so far no heavy-atom derivative that can lead to experimental phasing beyond 5-Å resolution has been found, and no marker or flag could be inserted into the electron density maps. Furthermore, it was shown that the undesirable properties of the H50S crystals become less tolerable with the increase in resolution. Hence, despite the fact that the current MIR with anomalous scattering map shows the overall structure of this particle and its main features, such as the exit tunnel (summarized by Yonath and Franceschi [1998]), as well as finer detail, traceable as RNA chains or ribosomal proteins, the prospects for solving the structure of this particle at molecular resolu-

tion are rather slim and depend on the development of new, innovative methods.

The packing diagram of the MIR with anomalous scattering map of H50S provides possible reasons for the odd combination of the properties of these crystals: high resolution accompanied by problematic diffraction. The high resolution may result from the extensive particle interactions that are concentrated in parts of the unit cell. In contrast, there is only a small interparticle contact area along the *c* axis (564 Å), which is surrounded by an extremely large solvent region. The small number of particle interactions may cause the poor isomorphism, the unfavorable crystal habit (plates, made of sliding layers, typically reaching up to 0.5 mm^2 with an average thickness of a few microns in the direction of the *c*-axis), and the variations in the *c*-axis length (567 to 570 Å) as a function of irradiation (Harms et al., 1999). It can also explain how very large clusters, such as those containing 30 tungsten atoms, 110 oxygens atoms, and 5 phosphate atoms $[K_{14}(NaP_5W_{30}O_{110})31H_2O]$, diffuse readily into the H50S crystals and why they may introduce subtle nonisomorphism and lead to limited and/or less reliable phase information. In order to facilitate structure determination, efforts aimed at increasing the level of isomorphism of the H50S crystals were made along the lines that were found suitable for T30S. These included inducing controlled rearrangements within the crystals by heat activation and treatment with selected additives, but neither led to significant improvement.

Crystals of T50S Diffract to 3.4 Å

In contrast to the H50S case, attempts at increasing the homogeneity of the crystallized T50S particle led most recently to a marked extension in resolution, from the previous limit of 9 to 10 Å to 3.4 Å. It should be mentioned that even when only low-resolution data could be obtained, the T50S crystals have been the target for crystallographic studies because of the high quality of their diffraction. Thus, Ta_6Br_{14}-soaked crystals led to two sites, readily extracted from isomorphous and anomalous-difference Patterson maps. These were used for initial single isomorphous replacement with anomalous phasing with the following final statistics: $R_{cullis} = 0.59$ (total) and 0.87 (anomalous) (R_{cullis} is defined as ⟨phase integrated lack of closure⟩/⟨$|F_{PH} - F_P|$⟩, where F_{PH} is the structure factor of the heavy-atom-derivatized crystals and F_P is that of the native protein); phasing power = 1.95; figure of merit (FOM)=0.58. In parallel, molecular replacement studies, performed with cryo-EM reconstructions of these particles, led to a unique solution that subsequently confirmed the main Ta_6Br_{14} sites (Fig. 6) (Harms et al., 1999). As these findings raise expectations for T50S structure determination, studies aimed at following the path of the nascent protein chains have been initiated. To shed light on the dynamic driving forces participating in the movement of newly born proteins, we co-crystallized complexes of T50S with short nascent polypeptides, along the same lines as for H50S (Berkovitch-Yellin et al., 1992), including the attachment of heavy atoms to the incorporated amino acids.

FUTURE PROSPECTS

We have shown that medium-resolution maps can be constructed for ribosomal particles, using experimental phases. These maps exhibit the external shapes and the internal features of the corresponding ribosomal particles, and for significant parts of them feasible interpretations at a level close to molecular resolution can be provided. Furthermore, selected locations on the ribosomal particles were revealed by covalently bound heavy-atom compounds. Thus, despite severe crystallographic problems, the way to structure determination has been paved and electron density maps at close to molecular resolution are emerging.

Intriguing questions associated with the functional flexibility of the small ribosomal subunit may be approached by the crystallization of particles at various conformational states, using tailor-made ligands, such as antibiotics or cDNA, to exposed single-stranded rRNA regions, or by letting these materials diffuse into the already-formed crystals. The observation that the conformation of the crystallized T30S particles is close to that of the active state in T30S has already led to the design of experiments aimed at obtaining higher-quality diffraction by further reactivation of the crystallized particles. Proceeding along these lines, and the examination of the changes in crystal behavior upon binding of selected ligands, should indicate the level of their involvement in functional recognition. Binding of metal compounds to these ligands should enable their unbiased positioning and provide indispensable information for map interpretation. Suitable examples, such as the freezing of the ribosomal structure by antibiotics, were mentioned above. Others will be based on the available biochemical information.

The extension of the resolution of T50S crystals, interesting and encouraging in their own rights, should make a noticeable impact on the future of ribosomal crystallography, since it opens the possibility

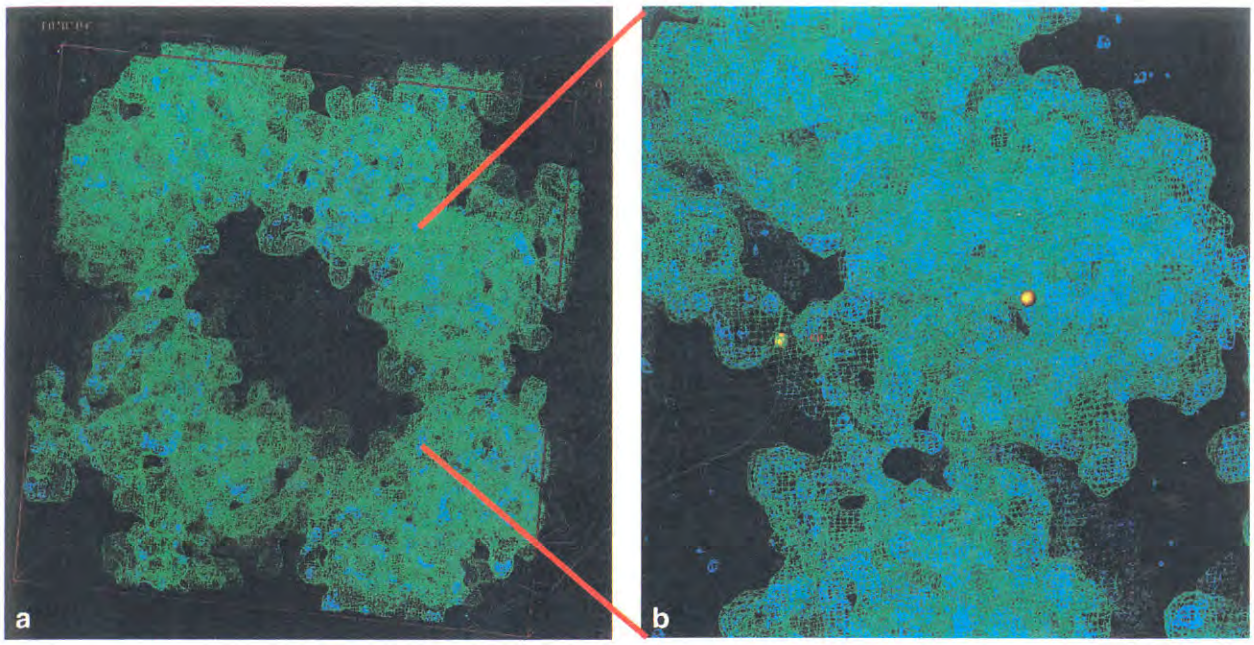

Figure 6. (a) Packing diagram of T50S, assembled by positioning the EM-reconstructed image (Yonath et al., 1998; Yonath and Franceschi, 1998; Harms et al., 1999) in the crystallographic unit cell according to the unique prominent result of the molecular replacement search. A total of 11,000 unique reflections (to 9-Å resolution) were collected from native and Ta_6Br_{14}-derivatized crystals. Six heavy-atom sites were extracted from anomalous-difference Patterson maps (FOM = 0.7188; R_{cullis} = 0.75; phasing power = 1.56). (b) The most prominent Ta_6Br_{14} sites are shown as golden balls (group scatterers with artificial diameters of about 6 Å).

of studying the three ribosomal particles from the same source, thus providing the tools for functional-structural comparisons. In the past we have grown crystals of T70S ribosomes diffracting to rather low resolution (20 to 24 Å) that was extended to 12 to 14 Å once the crystallized material was complexed with a 35-base RNA oligomer (as mRNA) and two charged tRNA molecules (Table 1) (Hansen et al., 1990). Since the packing arrangement of these crystals has been determined by molecular replacement (Harms et al., 1999) and since procedures that may lead to improvement in crystal quality have been developed, there is reason to expect improvement of T70S resolution too.

The growing popularity of ribosomal crystallography is indeed gratifying. This, together with the fruitful interactions with the exciting advances in cryo-EM, is bound to lead to major breakthroughs.

Thanks are given to M. Safro for active participation in phasing; M. Wilchek for indispensable advice; W. Jahn, W. Preetz, and M. Pope for their generous gifts of heavy-atom compounds; M. Van Heel, H. Stark, J. Frank, and I. Gabashvili for providing us with their cryo-EM reconstructions; W. Traub and A. Podjarny for fruitful discussions; and C. Radzwill, H. Burmeister, R. Albrecht, C. Glotz, J. Müssig, C. Paulke, M. Laschever, S. Meier, Y. Halfon, and K. Knaack for their excellent contributions in the different stages of these studies. Data were collected at the European Molecular Biology Laboratory and Max-Planck Society beam lines at The German Electron Synchrotron Facility; Station F1 at Cornell High Energy Synchrotron Source, Cornell University; Stations ID2 and ID13 at the European Synchrotron Radiation Facility, Grenoble, Spain; and Station ID19 at the Advanced Photon Source, Argonne National Laboratory.

Support was provided by the Max-Planck Society, the National Institutes of Health (NIH GM 34360), the German Ministry for Science and Technology (BMBF 05-641EA), and the Kimmelman Center for Macromolecular Assembly at the Weizmann Institute. A.Y. holds the Martin S. Kimmel Professorial Chair.

REFERENCES

Alexander, R. W., P. Muralikrishna, and B. S. Cooperman. 1994. Ribosomal components neighboring the conserved 518–533 loop of 16S rRNA in 30S subunits. *Biochemistry* 33:12109–12118.

Auerbach, T., T. Pioletti, H. Avila, K. Anagnostopoulos, S. Weinstein, F. Franceschi, and A. Yonath. Genetic and biochemical manipulation of the small ribosomal subunit from *T. thermophilus* HB8. *J. Biomol. Struct. Dyn.*, in press.

Ban, N., B. Freeborn, P. Nissen, P. Penczek, R. A. Graussucci, R. Sweet, F. Frank, P. Moore, and T. Steitz. 1998. The 9 Å resolution X-ray crystallography map of the large ribosomal subunits. *Cell* 93:1105–1115.

Basavappa, R., and P. B. Sigler. 1991. The 3-dimensional structure of yeast initiator tRNA: functional implication in initiator/elongator discrimination. *EMBO J.* 10:3105–3110.

Berkovitch-Yellin, Z., W. S. Bennett, and A. Yonath. 1992. Aspects in structural studies on ribosomes. *Crit. Rev. Biochem. Mol. Biol.* 27:403–444.

Brimacombe, R. 1995. The structure of ribosomal RNA; a three-dimensional jigsaw puzzle. *Eur. J. Biochem.* 230:365–383.

Camp, D., and W. E. Hill. 1987. Probing E. coli 16S ribosomal-RNA with DNA oligomers to determine functional and structural characteristics of the highly conserved G(530) loop. *FASEB J.* 46:2216–2221.

Capel, M. S., M. Kjeldgaard, D. M. Engelman, and P. B. Moore. 1988. Positions of S2, S13, S16, S17, S19 and S21 in the 30S ribosomal subunit of *E. coli. J. Mol. Biol.* 200:65–87.

Clemons, W. M., C. Davies, S. White, and V. Ramakrishnan. 1998. Conformational variability of the N-terminal helix in the structure of ribosomal protein S15. *Structure* 6:429–438.

Cusack, S. 1999. RNA protein complexes. *Curr. Opin. Struct. Biol.* 9:66–73.

Davies, C., V. Ramakrishnan, and S. W. White. 1996. Structural evidence for specific S8-RNA and S8-protein interactions within the 30S ribosomal subunit: ribosomal protein S8 from *B. stearothermophilus* at 1.9 Å resolution. *Structure* 4:1093–1104.

Draper, D. E., and L. P. Reynoldo. 1999. RNA binding strategies of ribosomal proteins. *Nucleic Acids Res.* 27:381–388.

Frank, F., J. Zhu, P. Penczek, Y. Li, S. Srivastava, A. Verschoor, M. Radermacher, R. Grassucci, A. R. Lata, and R. K. Agrawal. 1995. A model of protein synthesis based on cryo electron microscopy of the *E. coli* ribosome. *Nature* 376:441–444.

Gabashvili, I. S., R. K. Agrawal, R. Grassucci, and J. Frank. 1999. Structure and structural variations of the E. coli 30S ribosomal subunit as revealed by three-dimensional cryo-electron microscopy. *J. Mol. Biol.* 286:1285–1291.

Golden, B. L., D. W. Hoffman, V. Ramakrishnan, and S. W. White. 1993. Ribosomal protein S17: characterization of the three-dimensional structure by H and N NMR. *Biochemistry* 32: 12812–12820.

Guerin, M. F., and D. H. Hayes. 1987. Comparison of active and inactive forms of the E. coli 30S ribosomal subunits. *Biochimie* 69:965–974.

Hansen, H. A. S., N. Volkmann, J. Piefke, C. Glotz, S. Weinstein, I. Makowski, S. Meyer, H. G. Wittmann, and A. Yonath. 1990. Crystals of complexes mimicking protein biosynthesis are suitable for crystallographic studies. *Biochim. Biophys. Acta* 1050: 1–7.

Harms, J., A. Tocilj, I. Levin, I. Agmon, I. Kölln, H. Stark, M. van Heel, M. Cuff, F. Schlünzen, A. Bashan, F. Franceschi, and A. Yonath. 1999. Elucidating the medium resolution structure of ribosomal particles: an interplay between electron-cryo-microscopy and X-ray crystallography. *Structure* 7:931–941.

Hill, W. E., D. G. Camp, W. E. Tapprich, and A. Tassanakajon. 1988. Probing ribosomal structure and function using short oligo-deoxy-ribonucleotides. *Methods Enzymol.* 164:401–419.

Hosaka, H., A. Nakagawa, I. Tanaka, N. Harada, K. Sano, M. Kimura, M. Yao, and S. Wakatsuki. 1997. Ribosomal protein S7: a new RNA-binding motif with structural similarities to a DNA architectural factor. *Structure* 5:1199–1208.

Jahn, W. 1989. Synthesis of water soluble tetrairidium cluster for specific labelling of proteins. *Z. Naturforsch.* 44b:79–82.

Jones, T. A., J.-Y. Zou, S. W. Cowan, and M. Kjeldgaard. 1991. Improved methods for building protein models in electron density maps and the location of errors in these models. *Acta Crystallogr.* A47:110–119.

Krumbholz, S., F. Schlünzen, J. Harms, H. Bartels, I. Kölln, K. Knaack, W. S. Bennett, P. Bhanumoorthy, H. A. S. Hansen, N. Volkmann, A. Bashan, I. Levin, A. Tocilj, and A. Yonath. 1998. Ribosomal crystallography: cryo protectants and cooling agents. *Periodicum Biologorum* 100:119–125.

Lata, A. R., R. K. Agrawal, P. Penczek, R. Grassucci, J. Zhu, and J. Frank. 1996. Three-dimensional reconstruction of the E. coli 30S ribosomal subunit in ice. *J. Mol. Biol.* 262:43–52.

Liljas, A., and S. Al-Karadaghi. 1997. Structural aspects of protein synthesis. *Nat. Struct. Biol.* 4:767–771.

Lindhal, M., L. A. Svensson, A. Liljas, S. E. Sedelnikova, I. Eliseukina, N. Fomenkova, N. Nevskaya, S. Nikonov, N. Garber, and T. A. Muranova. 1994. Crystal structure of the ribosomal protein S6 from *T. thermophilus. EMBO J.* 13:1249–1254.

Malhotra, A., P. Penczek, R. K. Agrawal, I. S. Gabashvili, R. A. Grassucci, R. Junemann, N. Burkhardt, K. H. Nierhaus, and J. Frank. 1998. E. coli 70S ribosome at 15 A resolution by cryo-electron microscopy: localization of fMet-tRNA$_f^{Met}$ and fitting of L1 protein. *J. Mol. Biol.* 280:103–115.

Moazed, D., and H. F. Noller. 1987. Interaction of antibiotics with functional sites in 16S ribosomal RNA. *Nature* 327:389–394.

Mueller, F., and R. Brimacombe. 1997. A new model of the three-dimensional folding of *E. coli* 16S ribosomal RNA. II. The RNA-protein interaction data. *J. Mol. Biol.* 271:524–544.

Nevskaya, N., S. Tishchenko, A. Nikulin, S. Al-Karadaghi, A. Liljas, B. Ehresmann, C. Ehresmann, M. Garber, and S. Nikonov. 1998. Crystal structure of ribosomal protein S8 from Thermus thermophilus reveals a high degree of structural conservation of a specific RNA binding site. *J. Mol. Biol.* 279:233–244.

Oakes, M. I., M. W. Clark, E. Henderson, and J. A. Lake. 1986. DNA hybridization electron microscopy: ribosomal RNA nucleotides 1392–1407 are exposed in the cleft of the small subunit. *Proc. Natl. Acad. Sci. USA* 83:275–279.

Ramakrishnan, V., and S. W. White. 1992. The structure of ribosomal protein S5 reveals sites of interaction with 16S RNA. *Nature* 358:768–771.

Ramakrishnan, V., and S. W. White. 1998. Ribosomal protein structures: insights into the architecture, machinery and evolution of the ribosome. *Trends Biochem. Sci.* 3:208–212.

Richmond, T. J., J. T. Finch, B. Rushton, D. Rhodes, and A. Klug. 1984. Structure of the nucleosome core particle at 7 Å resolution. *Nature* 311:532–537.

Ricker, R. D., and A. Kaji. 1991. Use of single strand DNA oligonucleotide in programming ribosomes for translation. *Nucleic Acids Res.* 19:6573–6578.

Sagi, I., V. Weinrich, I. Levin, C. Glotz, M. Laschever, M. Melamud, F. Franceschi, S. Weinstein, and A. Yonath. 1995. Crystallography of ribosomes: attempts at decorating the ribosomal surface. *Biophys. J.* 55:31–41.

Schluenzen F., H. A. S. Hansen, J. Thygesen, W. S. Bennett, N. Volkmann, I. Levin, J. Harms, H. Bartels, A. Bashan, Z. Berkovitch-Yellin, I. Sagi, F. Franceschi, S. Krumbholz, M. Geva, S. Weinstein, I. Agmon, N. Boeddeker, S. Morlang, R. Sharon, A. Dribin, M. Peretz, V. Weinrich, and A. Yonath. 1995. A milestone in ribosomal crystallography: the construction of preliminary electron density maps at intermediate resolution. *J. Biochem. Cell Biol.* 73:739–749.

Schluenzen, F., M. Gluehmann, D. Janell, I. Levin, A. Bashan, J. Harms, H. Bartels, T. Auerbach, T. Pioletti, H. Avila, K. Anagnostopoulos, H. A. S. Hansen, W. S. Bennett, I. Agmon, M. Kessler, A. Tocilj, M. Peretz, S. Weinstein, F. Franceschi, and A. Yonath. 1999. The identification of selected components in electron density maps of prokaryotic ribosomes at 7 Å resolution. *J. Synth. Radiat.* 6:928–941.

Stark, H., F. Mueller, E. V. Orlova, M. Schatz, P. Dube, T. Erdemir, F. Zemlin, R. Brimacombe, and M. van Heel. 1995. The 70S *E. coli* ribosome at 23 Å resolution: fitting the ribosomal RNA. *Structure* 3:815–821.

Stöffler, G., and M. Stöffler-Meilicke. 1986. Immuno electron microscopy on E. coli ribosomes, p. 28–46. *In* B. Hardesty and G. Kramer (ed.) *Structure, Function and Genetics of Ribosomes.* Springer Verlag, Heidelberg, Germany.

Szer, W., and Z. Kurylo-Borowska. 1972. Interactions of edeine with bacterial ribosomal subunits. Selective inhibition of ami-

noacyl-tRNA binding sites. *Biochem. Biophys. Acta* 259:357–368.

Tanaka, I., A. Nakagawa, H. Hosaka, S. Wakatsuki, F. Mueller, and R. Brimacombe. 1998. Matching the crystallographic structure of ribosomal protein S7 to the 3D model of 16S RNA. *RNA* 4:542–550.

Tapprich, W. E., and W. E. Hill. 1986. Involvement of bases 787–795 of E. coli 16S RNA in ribosomal subunit association. *Proc. Natl. Acad. Sci. USA* 83:556–560.

Trakhanov, S. D., M. M. Yusupove, V. A. Shirokov, M. B. Garber, A. Mitscher, M. Ruff, J.-C. Tierry, and D. Moras. 1989. Preliminary X-ray investigation on 70S ribosome crystals. *J. Mol. Biol.* 209:327–334.

Van Heel, M., and H. Stark. Unpublished data.

Volkmann, N., S. Hottentrager, H. A. S. Hansen, A. Zaytzev-Bashan, R. Sharon, Z. Berkovitch-Yellin, A. Yonath, and H. G. Wittmann. 1990. Characterization and preliminary crystallographic studies on large ribosomal subunits from Thermus thermophilus. *J. Mol. Biol.* 216:239–243.

von Böhlen, K., I. Makowski, H. A. S. Hansen, H. Bartels, Z. Berkovitch-Yellin, A. Zaytzev-Bashan, S. Meyer, C. Paulke, F. Franceschi, and A. Yonath. 1991. Characterization and preliminary attempts for derivatization of crystals of large ribosomal subunits from Haloarcula marismortui, diffracting to 3 Å resolution. *J. Mol. Biol.* 222:11–15.

Wada, T., T. Yamazaki, S. Kuramitsu, and Y. Kyogoku. 1999. Cloning of the RNA polymerase alfa subunit gene from Thermus thermophilus HB8 and characterization of the protein. *J. Biochem.* 125:143–150.

Weinstein, S., W. Jahn, C. Glotz, F. Schlünzen, I. Levin, D. Janell, J. Harms, I. Kölln, H. A. S. Hansen, M. Glühmann, W. S. Bennett, H. Bartels, A. Bashan, I. Agmon, M. Kessler, M. Pioletti, H. Avila, K. Anagnostopoulos, M. Peretz, T. Auerbach, F. Franceschi, and A. Yonath. 1999. Metal compounds as tools for the construction and the interpretation of medium resolution maps of ribosomal particles. *J. Struct. Biol.* 127:141–151.

Weller, J. W., and W. E. Hill. 1992. Probing dynamic changes in rRNA conformation in the 30S subunit of the E. coli ribosome. *Biochemistry* 31:2748–2757.

Wimberly, B.T., S. W. White, and V. Ramakrishnan. 1997. The structure of ribosomal protein S7 at 1.9 Å resolution reveals a beta-hairpin motif that binds double-stranded nucleic acids. *Structure* 5:1187–1198.

Yonath, A., and F. Franceschi. 1998. Functional universality and evolutionary diversity: insights from the structure of the ribosome. *Structure* 6:678–684.

Yonath, A. C. Glotz, H. S. Gewitz, K. Bartels, K. von Boehlen, I. Makowski, and H. G. Wittmann. 1988. Characterization of crystals of small ribosomal subunits, *J. Mol. Biol.* 203:831–833.

Yonath, A., J. Harms, H. A. S. Hansen, A. Bashan, M. Peretz, H. Bartels, F. Schluenzen, I. Koelln, W. S. Bennett, I. Levin, S. Krumbholz, A. Tocilj, S. Weinstein, I. Agmon, M. Piolleti, T. Auerbach, and F. Franceschi. 1998. The quest for the molecular structure of a large macromolecular assembly exhibiting severe non-isomorphism, extreme beam sensitivity and no internal symmetry. *Acta Crystallogr.* 54A:945–955.

Zamir, A., R. Miskin, and D. Elson. 1971. Inactivation and reactivation of ribosomal subunits: amino acyl-transfer RNA binding activity of the 30S subunits of E. coli. *J. Mol. Biol.* 60:347–364.